Global and Planetary Change 161 (2018) 53–65

Contents lists available at ScienceDirect

Global and Planetary Change

journal homepage: www.elsevier.com/locate/gloplacha

A nonparametric standardized runoff index for characterizing hydrological drought on the Loess Plateau, China

Jingwen Wu[a], Chiyuan Miao[a,*], Xu Tang[a], Qingyun Duan[a], Xiaojia He[b]

[a] State Key Laboratory of Earth Surface Processes and Resource Ecology, Faculty of Geographical Science, Beijing Normal University, Beijing 100875, China
[b] The Administrative Center for China's Agenda21, Beijing 100038, China

ARTICLE INFO

Editor: Dr. Sierd Cloetingh

Keywords:
Hydrological drought
NSRI
Loess Plateau
ENSO
Cross-wavelet analysis

ABSTRACT

Drought is one of the world's most recurrent and destructive hazards, and the evolution of drought events has become increasingly complex against a background of climate change and changing human activities. Over the last five decades, there have been frequent droughts on the Loess Plateau in China. In this study, we used the nonparametric standardized runoff index (NSRI) to investigate the temporal characteristics of hydrological drought in 17 Loess Plateau catchments during the period 1961–2013. Furthermore, we used a cross-wavelet transform to reveal linkages between an El Niño-Southern Oscillation (ENSO) index and the NSRI series. The primary results indicated that the annual and seasonal NSRI series displayed statistically significantly downward trends in all catchments, with the only exception being the winter NSRI series in Yanhe. Furthermore, our analyses showed downward trends persisting into the future in all 17 catchments except Yanhe. We also found that, overall, the risk of hydrological drought was high on the Loess Plateau, with the mean duration at the seasonal scale exceeding 4 months and the mean duration at the annual scale exceeding 12 months. Moreover, during recent years, the trend towards hydrological drought was greater in the spring than in other seasons. ENSO events were closely associated with annual and seasonal hydrological drought on the Loess Plateau, and the impact of ENSO events was stronger in the southeast of the plateau than the northwest at both seasonal and annual scales. These results may provide valuable information about the evolutionary characteristics of hydrological drought across the Loess Plateau and may also be useful for predicting and mitigating future hydrological drought on the plateau.

1. Introduction

Recurrent drought is one of the most damaging natural hazards and has attracted considerable attention from meteorologists, agriculturalists, hydrologists, and ecological scientists (Mishra and Singh, 2010). Droughts have had clear adverse impacts on socio-economic development and ecological conditions around the world (Liu et al., 2012; Van Loon and Laaha, 2015; Yang et al., 2017c), and such impacts are expected to increase in severity as a result of changing climates (Huang et al., 2016). Drought can be subdivided into four types according to different variables in the hydrological cycle: meteorological drought, reflected by changes in precipitation and evapotranspiration (ZP Liu et al., 2016), agricultural drought, reflected by changes in soil moisture (Zargar et al., 2011), socioeconomic drought, reflected by the degree of water availability (Gao et al., 2014b; Van Loon and Laaha, 2015), and hydrological drought, reflected by changes in runoff and groundwater (Tallaksen et al., 2004; Wada et al., 2013). When a meteorological drought propagates for a period of time, the lack of precipitation results in decreased soil moisture and river flow, which eventually leads to agricultural and hydrological droughts (Yuan et al., 2016). Almost all human activities (e.g. irrigation, urban and industrial activities) are highly dependent on water resources from surface runoff and groundwater (Huang et al., 2016), thus hydrological drought is considered a very important category of drought. Global climate change has intensified the global hydrological cycle in recent years (Miao et al., 2016; Y Gao et al., 2016; Liu et al., 2017) and the frequency of hydrological drought may continue to increase owing to global warming (Huang et al., 2016; X Liu et al., 2016).

Hydrological droughts have a widespread impact and affect a diverse array of economic and social activities. For example, hydrological droughts reduce water supply and power generation, restrict water for irrigation (causing crop failure), disturb riparian habitats, cause a deterioration in water quality, and so on (Mishra and Singh, 2010). During the last few decades, studies have been published regarding hydrological drought for a number of regions all over the world. However, the characteristics and mechanisms influencing hydrological

* Corresponding author.
E-mail address: miaocy@bnu.edu.cn (C. Miao).

https://doi.org/10.1016/j.gloplacha.2017.12.006
Received 6 June 2017; Received in revised form 24 October 2017; Accepted 6 December 2017
Available online 08 December 2017
0921-8181/ © 2017 Elsevier B.V. All rights reserved.

drought are diverse because of the degree of variety in ecological environments and climatic conditions. Indeed, within a single climate region, hydrological drought characteristics can vary according to basin properties (Van Lanen et al., 2004; Gao et al., 2014a). Thus, a deep understanding of the risk and evolutionary characteristics of hydrological drought within a single climate region is essential: such studies can elucidate the evolutionary characteristic and underlying mechanisms of hydrological drought, enhancing adaptive capacity and mitigating the potential impacts of hydrological drought.

Different variables involved in the water cycle can characterize hydrological drought, such as streamflow, groundwater, and reservoir storage. However, the results of drought analysis may differ substantially as focus shifts among the different variables. Hydrologists often use streamflow (or runoff) to denote hydrological drought because of its rapid response to meteorological drought (Tallaksen et al., 2004; Yang et al., 2017b). Hydrological drought indices are the simplest and most frequently used approach because they provide an objective, quantitative assessment of various drought characteristics (e.g. magnitude, duration, and intensity) (Tabari et al., 2013). In recent decades, many hydrological drought indices have been developed (Dracup et al., 1980; Tallaksen et al., 2004; Shukla and Wood, 2008; Farahmand and AghaKouchak, 2015). Shafer and Dezman (1982) designed the Surface Water Supply Index (SWSI), which incorporates multiple hydro-meteorological variables (e.g. precipitation, runoff, snowpack, and reservoir storage), to complement the Palmer Drought Severity Index (PDSI) for moisture conditions across the state of Colorado. Their results indicated the frequency of occurrence of mild, moderate, and severe drought at 26%–50%, 14%–26%, and 2%–14%, respectively. The Aggregate Drought Index (ADI) was designed by Keyantash and Dracup (2004) and takes all physical forms of drought into account by using a wide range of variables (e.g. streamflow, soil moisture, precipitation, snow water content, and pan evaporation). The ADI was evaluated in three different climate divisions in California, and the results showed that it successfully delineated two dominant droughts in California (the 1976–1977 and 1987–1992 droughts) with severities and magnitudes qualitatively consistent with the recorded event severities. Fleig et al. (2011) developed the Regional Drought Area Index (RDAI) using daily streamflow to describe the drought characteristics in northwestern Europe. The RDAI denoted severe drought events in all regions in 1976 and 1996; observed data shows that those years had the most severe drought in the study period. Shukla and Wood (2008) proposed the standardized runoff index (SRI), which uses runoff data and is analogous to the standardized precipitation index (SPI) (McKee et al., 1993). They tested the efficacy of the SRI in Feather River basin and showed it was useful for depicting hydrological aspects of drought. Farahmand and AghaKouchak (2015) developed nonparametric univariate and multivariate standardized indices that could be applied to different variables including precipitation, soil moisture, runoff, etc. This method is particularly favorable for drought assessments that use multiple drought indicators. In brief, most existing drought indicators rely on a representative parametric distribution function to fit the data in terms of shape, skewness, and kurtosis. This can lead to various tail behaviors, especially at the local scale (Farahmand and AghaKouchak, 2015). Therefore, a nonparametric drought index fills a major gap in drought-related studies (Huang et al., 2015).

The evolutionary characteristics of hydrological droughts do not generally follow a set of fixed spatiotemporal patterns (Huang et al., 2016). Changes in climate may contribute to this variability. Analysis of the links between hydrological droughts and climate indices therefore has the potential to reveal important information about the hydro-climatological mechanisms driving the development of hydrological droughts (Fleig et al., 2011). Ryu et al. (2010) explored the relationship between the El Niño Southern Oscillation (ENSO) and hydrological drought in the United States, and found negative relationships in southern California and the northern Great Plains, but positive relationships in the Pacific Northwest (Oregon, Washington, and northern California). Talaee et al. (2014) analyzed the possible association between large-scale atmospheric circulation patterns and hydrological droughts in the western region of Iran. They found an effect of ENSO teleconnections on the severity of the hydrological drought in 1969–1970, especially between November and March. YX Wang et al. (2015) investigated the effects of large-scale climate patterns on hydrological drought in the Luanhe River basin in China. They observed a significant influence of the Atlantic Multidecadal Oscillation (AMO) on hydrological drought at different time scales, with warm AMO phases conducive to drought conditions. Huang et al. (2016) employed a cross-wavelet analysis to reveal the correlations between hydrological drought and monthly climate indices in the Columbia River basin. Their results indicated that the ENSO and the Arctic Oscillation (AO) play a major role in hydrological drought in that region, with the ENSO primarily affecting hydrological drought at a relatively short time scale (2–7 years) but the AO having effects at a relatively longer time scale ($>$ 10 years).

The Loess Plateau is situated in the upper and middle reaches of China's second-largest river (the Yellow River). It has been an important agricultural district in China for thousands of years and currently benefits 114 million people, or 8.5% of the total population of China (Kong et al., 2016). Owing to a complex set of factors including the unique climatic conditions, the particular geographic landscape, and intensive human activities, the Loess Plateau has suffered serious water erosion of the soil resulting in an enormous sediment discharge in the Yellow River (i.e. relatively low streamflow discharge yet huge sediment load) (Miao et al., 2011; Wu et al., 2017). In order to control the serious erosion of the Loess Plateau, a number of soil and water conservation measures have been implemented during the last five decades. Combined with the impacts of the changing climate, this has resulted in complex drought conditions across the plateau (ZP Liu et al., 2016). Therefore, a comprehensive investigation of the drought characteristics in this important region will be indispensable in order to guarantee food security in the region and sustainable development of the ecological environment. ZP Liu et al. (2016) used the Standardized Precipitation Index (SPI) and the Standardized Precipitation Evapotranspiration Index (SPEI) to identify the spatiotemporal characteristics of drought conditions between 1957 and 2012 and found an upward trend in drought severity. Zhao and Wu (2013) used the PDSI to identify drought conditions on the Loess Plateau over the period 1971–2010 and found that most regions exhibited spatially increasing trends in drought severity and frequency. LN Wang et al. (2015) used the drought threshold method to explore drought trends and the relationship with rainfall intensity. They found an overall upward trend in the frequency of drought occurrence on the Loess Plateau during the period 1961–2012 and, moreover, an increase in drought magnitude and a decrease in the probability of heavy and extraordinary rainstorms.

These previous studies mostly focused on the evolutionary characteristics of meteorological drought on the Loess Plateau, there has been no analysis of hydrological drought in the region to date. In addition, most previous drought analyses in this region did not take into consideration the effect of teleconnections such as the ENSO. Thus, our study fills in the gaps in our knowledge of hydrological drought on the Loess Plateau, and provides a deeper understanding of the evolutionary characteristics and mechanisms influencing drought in the region. Moreover, against a regional background of decreasing water resource and fragile ecological environment (Liang et al., 2015), our study will aid the implementation of scientific water-resource management and the return of ecological balance to the Loess Plateau. The results of this study will likely also benefit the development of reasonable policies to mitigate the effects of drought and guarantee food security.

The main objectives of this study are: (1) to characterize hydrological drought (drought duration, intensity) in 17 catchments on the Loess Plateau; (2) to fully reveal the evolutionary characteristics (trends, persistence) of seasonal and annual hydrological drought; (3) to explore the contributions of seasonal hydrological drought to annual

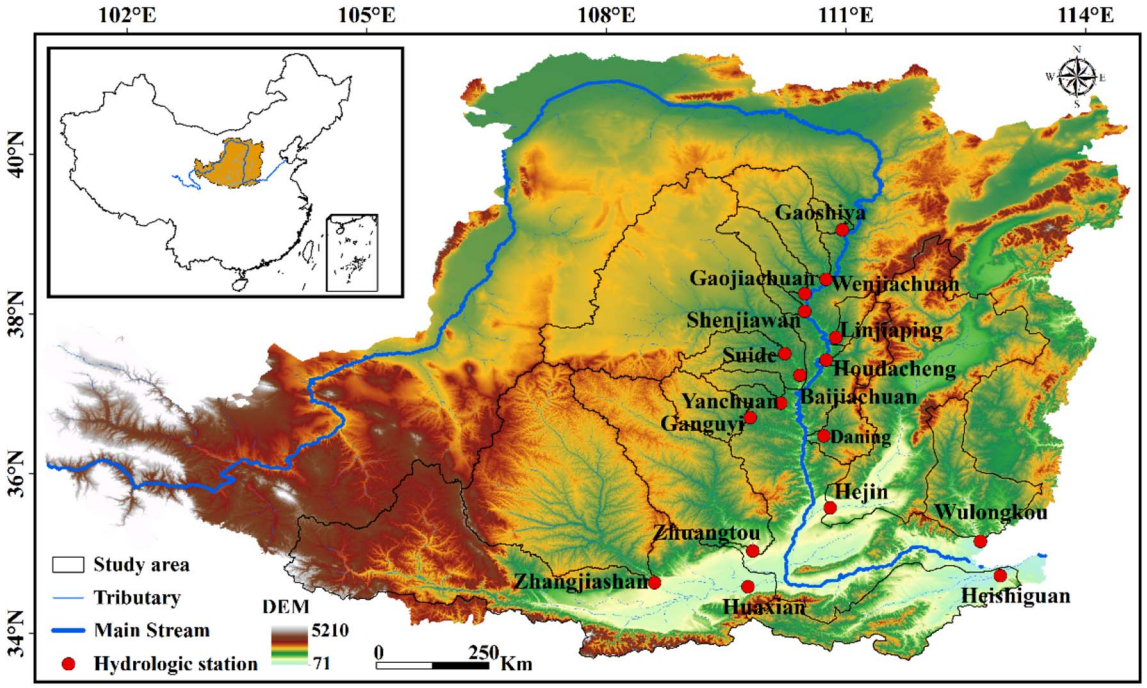

Fig. 1. Geographic location of the 17 catchments and hydrological stations used in this study.

hydrological drought; (4) to capture the influence of the El Niño-Southern Oscillation (ENSO) on hydrological drought.

2. Study area and data

The Loess Plateau (35°N–41°N, 102°E–114°E) is located in the upper and middle reaches of the Yellow River in Northwest China (Fig. 1). It covers an area of approximately 640,000 km^2, accounting for 6.6% of the total area of Chinese land, and sustains 8.5% of the Chinese population (Fu et al., 2011). The plateau lies in the marginal area of the East Asian and South Asian summer monsoons and is seriously influenced by monsoon activity and intensity. The multi-year mean temperature is approximately 9.0 °C, ranging from 3.6 °C in the northwest to 14.3 °C in the southeast. There are distinct seasonal changes, with a dry and cold winter, rapidly rising temperatures in spring, a hot and humid summer, and rapidly lowering temperatures in autumn. The multi-year mean precipitation is about 420 mm, ranging from 200 mm in the northwest to 750 mm in the southeast, and the precipitation mainly falls from June to September in high intensity storms (i.e. 60%–70% of the total precipitation falls at this time). Because of deforestation and cultivation, the natural vegetation in the region has been largely destroyed. Owing to its unique climatic features and poor vegetation coverage, the Loess Plateau is one of the most water-deficient region in China: the amount of water available per capita on the Loess Plateau region is only one-fifth of the national average, and the water availability for cultivated land is less than one-eighth of the national average (Zhang and Schwärzel, 2017). For many years, this region was notorious for severe drought, soil erosion, sparse vegetation, and high population pressure (Wang et al., 2017). Since the 1950s, the Chinese government has implemented a series of ecological restoration measures on the Loess Plateau to prevent severe soil erosion. The increased vegetation cover intercepts precipitation, increases evapotranspiration, improves the infiltration rate, and slows or retains runoff; thus there is now a significant downward trend in runoff in the region.

The sub-basins in the Loess Plateau have strong climate and land surface gradients (Liang et al., 2015); moreover, hydrological drought characteristics vary according to basin properties (Fleig et al., 2011). Thus, we selected 17 primary watersheds located in this region as representative, and used these to reveal the evolutionary characteristics of hydrological drought on the Loess Plateau. These 17 catchments cover approximately 44.5% of the entire area of the Loess Plateau, but together contribute about 77.7% of total runoff and about 88.6% of sediment discharge from the Loess Plateau. Details of the 17 catchments are shown in Table 1.

Monthly runoff data during the period 1961–2013 for 17 hydrological stations on the Loess Plateau were obtained from the Yellow River Conservancy Commission (YRCC). Annual and seasonal (i.e. spring, summer, autumn, and winter) hydrological droughts were explored with these data. Spring, summer, autumn, and winter were defined as March to May, June to August, September to November, and December to February, respectively. We characterized ENSO events using the monthly Nino 3.4 Index data for the period 1960–2008 acquired from the NOAA Earth System Research Laboratory (http://www.esrl.noaa.gov/psd/data/correlation/nina34.data).

3. Methodology

In this study, a nonparametric standardized runoff index was used to characterize hydrological drought (e.g. drought duration and drought intensity) in 17 catchments on the Loess Plateau. The Mann-Kendall (MK) trend test method and rescaled range (R/S) analysis were used to characterize the trends in hydrological drought over the last five decades and in near future. With these methods, we obtained general hydrological drought characteristics for the 17 plateau catchments. We then used variance decomposition to capture the contributions of changes in seasonal hydrological drought to changes in annual hydrological drought, and cross-wavelet analysis to investigate the linkages between the ENSO and hydrological drought at the seasonal and annual scales. These two methods allow us to obtain a deeper understanding of the underlying mechanisms and evolutionary characteristics of the hydrological drought on the Loess Plateau.

3.1. Nonparametric standardized runoff index (NSRI)

In this study, a nonparametric standardized runoff index (NSRI) was used to characterize hydrological drought. Compared with the original

Table 1
Detailed summary of the hydrological variables associated with the 17 Loess Plateau catchments.

ID	Catchment	Gauging station	Area (km^2)	Long-term annual mean runoff value (1961–2013) (unit: mm)				
				Spring	Summer	Autumn	Winter	Annual
GSCH	Gushanchuan	Gaoshiya	1260	7.49	31.34	8.49	1.17	48.48
KYH	Kuye	Wenjiachuan	8621	12.95	27.24	13.06	5.22	58.36
TWH	Tuwei	Gaojiachuan	4955	23.22	26.73	24.49	19.9	93.97
WDH	Wuding	Baijiachuan	44,683	8.42	10.51	9.49	7.32	35.59
JLH	Jialu	Shenjiawan	1138	10.23	21.78	10.92	5.94	48.77
DLH	Dali	Suide	3861	6.75	16.39	8.13	4.41	35.59
QJH	Qingjian	Yanchuan	2095	6.09	20.37	8.54	3.53	38.46
YH	Yanhe	Ganguyi	5857	6.08	17.88	7.57	3.18	34.64
BLH	Beiluo	Zhuangtou	25,723	5.85	10.65	9.12	3.64	29.19
JLH	Jinghe	Zhangjiashan	43,106	5.67	14.09	10.65	3.57	33.92
WH	Weihe	Huaxian	63,205	10.71	19.52	25.91	5.03	61.08
YLH	Yiluo	Heishiguan	18,707	20.84	41.61	48.77	17.47	128.35
QSH	Qiushui	Linjiaping	2015	4.04	21.07	7.08	2.04	34.2
SCH	Sanchuan	Houdacheng	4027	8.83	20.34	14.16	7.37	50.56
FH	Fenhe	Hejin	39,199	2.56	7.6	8.13	3.59	21.82
XSH	Xinshui	Daning	3992	3.71	14.26	8.26	2.8	28.98
QH	Qinhe	Wulongkou	12,596	9.58	30.95	29.79	10.13	80.25

standard runoff index (SRI) in which a monthly runoff series is fit with a Pearson III distribution (Vicente-Serrano et al., 2012), the NSRI series is derived from an empirical probability distribution. The marginal probability of runoff is derived from the empirical Gringorten plotting position (Gringorten, 1963):

$$P(x_j) = \frac{i - 0.44}{n + 0.12} \tag{1}$$

where n represents the runoff size, i indicates the rank of non-zero runoff data from smallest to largest, and $P(x_j)$ is the corresponding empirical probability at month j. Then the calculated empirical probabilities can be transformed into a standardized index (SI) as follows:

$$SI = \varnothing^{-1}(p) \tag{2}$$

where $\varnothing$ represents the standard normal distribution function and p indicates the probability derived from Eq. (1). We can also calculate Eq. (2) from the following commonly-used approximation:

$$SI = \begin{cases} -\left(t - \frac{c_0 + c_1 t + c_2 t^2}{1 + d_1 t + d_2 t^2 + d_3 t^3}\right) & 0 < p \le 0.5 \\ +\left(t - \frac{c_0 + c_1 t + c_2 t^2}{1 + d_1 t + d_2 t^2 + d_3 t^3}\right) & 0.5 < p \le 1 \end{cases} \tag{3}$$

$$t = \begin{cases} \sqrt{\ln \frac{1}{p^2}} & 0 < p \le 0.5 \\ \sqrt{\ln \frac{1}{(1-p)^2}} & 0.5 < p \le 1 \end{cases} \tag{4}$$

where $c_0 = 2.515517$, $c_1 = 0.802583$, $c_2 = 0.010328$, $d_1 = 1.432788$, $d_2 = 0.189369$, and $d_3 = 0.001308$.

3.2. Drought identification

Severity, duration, and intensity are regarded as the three most important parameters characterizing a drought event (Huang et al., 2016). In this study, drought duration was defined as the length of time during which the NSRI was below a specific threshold. Drought severity was defined as the total deficit in NSRI values in a single drought event. Drought intensity was defined as the ratio of drought severity to drought duration. As severity, duration, and intensity are closely related, any two are sufficient to depict a specific drought event (Sadeghipour and Dracup, 1985). Thus, in this study, we selected drought intensity and drought duration. A threshold of −0.8 is often chosen to represent drought conditions in hydrological drought analyses (Hao and AghaKouchak, 2013; Yuan et al., 2016). An NRSI value below −0.8 for more than three consecutive months is commonly used to indicate a single drought event (Yuan and Wood, 2013).

To better understand the evolutionary characteristics of hydrological drought, hydrological drought needs to be investigated at different scales. In this study, hydrological drought was evaluated according to NSRI at 3-month (NSRI-3) and 12-month time scales (NSRI-12). The runoff data on the "moving windows" of 3 and 12 months was averaged to calculated NSRI-3 and NSRI-12 respectively. For example, when calculating the NSRI-3 aimed at January–March in 1970, we firstly fitted an empirical distribution based on 3–month moving average runoff, and then the mean runoff during January–March in 1970 corresponded the NSRI-3 in the same period. Therefore, we used the NSRI-3 values focused on March–May, June–August, September–November, and December–February during the period 1961–2013 to characterize spring, summer, autumn, and winter hydrological drought conditions, respectively. Similarly, the NSRI-12 values focused on January–December were used to characterize annual hydrological drought. These two time scales can characterize short-term and long-term hydrological drought conditions, respectively (Ren et al., 2016).

3.3. Mann-Kendall (MK) trend test method

The non-parametric Mann-Kendall (MK) test has been widely employed in environmental, climate, and hydrological studies (Gocic and Trajkovic, 2013). The sample data must be serially independent, otherwise the significance of the trend is inaccurate (Yue et al., 2002). Therefore, we first used the method introduced by Yue et al. (2002) to remove autocorrelation in the time series, and then we carried out the main test according to Sun et al. (2014) and Yue et al. (2002). The process was as follows:

Eliminate the trend in the time series and divide the original time series into a trend series and a residual series:

$$\dot{y}_t = y_t - T_t = y_t - \beta \times t \tag{5}$$

$$\beta = \text{median}\left(\frac{y_j - y_i}{j - i}\right) \tag{6}$$

The parameters of the autoregressive (AR) model for the residual time series are calculated as:

$$l_k = \frac{\sum_{i=1}^{n-k} (y_i - y)(y_{i+k} - \bar{y})}{\sum_{i=1}^{n} (y_i - y)^2} \tag{7}$$

β is the median of all combinations of record pairs for the entire data sample, n is the length of the data sample, l_k is the lag-k autocorrelation efficient, and $\bar{y}$ is the mean. Then, the AR (1) component is eliminated from the time series by the following equation:

$$\ddot{y}_t = \dot{y}_t - l_1 \times \dot{y}_{t-1} \tag{8}$$

After the AR component has been eliminated from the trend, the series is recombined:

$$\ddot{y}_t = \ddot{y}_t + T_t \tag{9}$$

where $\ddot{y}_t$ denotes the dataset with the corrected trend. The MK test is then applied to the new series $\ddot{y}_t$. The MK test statistic Z is given by:

$$Z = \begin{cases} \frac{S-1}{\sqrt{Var(S)}}, & if\ S > 0 \\ 0, & if\ S > 0 \\ \frac{S+1}{\sqrt{Var(S)}}, & if\ S > 0 \end{cases} \tag{10}$$

where

$$S = \sum_{i=1}^{n-1} \sum_{j=i+1}^{n} sig(x_j - x_i) \tag{11}$$

$$sig(x_j - x_i) = \begin{cases} 1, & if\ (x_j - x_i) > 0 \\ 0, & if\ (x_j - x_i) = 0 \\ -1, & if\ (x_j - x_i) < 0 \end{cases} \tag{12}$$

$$Var(S) = \left[n(n-1)(2n+5) - \sum_{i=1}^{m} t_k (t_k - 1)(2t_k + 5) \right] / 18 \tag{13}$$

where x is the new series $\ddot{y}_t$, x_j and x_i are the observations in chronological order, m is the number of tied values, $t_k$is the number of ties for kth value, $sig(x_j - x_i)$ is the sign function, and $Var(S)$ is the variance of the statistic S. In our study, trend significance was tested at the $\alpha = 0.05$ $(1.96 \le |Z| < 2.58)$ and $\alpha = 0.01$ $(|Z| \ge 2.58)$ significance levels. Positive values of Z denote upward trends across the entire time series, whereas negative values of Z denote downward trends across the entire time series.

3.4. Rescaled range (R/S) analysis

The R/S analysis was initially proposed by Hurst, a British hydrologist, in 1951 when he investigated fluctuations in the water level in the Nile River (Hurst, 1951). Since then, R/S analysis has been widely used in many fields, including finance, cardiology, morphology, and hydrology (Wang et al., 2013). The basic theory of the R/S analysis can be described as follows:

For the time series of a certain variable $x(t)$, $t = 1, 2, 3\ldots\ldots n$, the average value of $x(t)$ is defined as:

$$x(\varepsilon) = \frac{1}{\varepsilon} \sum_{t=1}^{\varepsilon} x(t) \quad \varepsilon = 1, 2, 3\ldots\ldots \tag{14}$$

The cumulative deviation is:

$$F(t, \varepsilon) = \sum_{k=1}^{t} (x(k) - x(\varepsilon)) \tag{15}$$

The range sequence is:

$$R(\varepsilon) = \max_{1 \le t \le \varepsilon} F(t, \varepsilon) - \min_{1 \le t \le \varepsilon} F(t, \varepsilon) \quad F(t, \varepsilon) = 1, 2, 3\ldots\ldots \tag{16}$$

The standard deviation is:

$$S(\varepsilon) = \left[\frac{1}{\varepsilon} \sum_{t=1}^{\varepsilon} (x(t) - x(\varepsilon)^2) \right]^{1/2} \quad \varepsilon = 1, 2, 3\ldots\ldots \tag{17}$$

Then the dimensionless ratio R/S is defined as:

$$R/S = (\alpha\varepsilon)^H \quad (\alpha \text{ is a constant}) \tag{18}$$

Hurst reported $\ln(R/S)$ and $\ln(\varepsilon)$ and found that the points lie almost on a straight line with excellent regularity (Shi et al., 2013). The slope of the line is the Hurst Exponent (H). Different H values denote different trends in the time series. $H = 0.5$ indicates that the sequence is an independent random process; $0 < H < 0.5$ indicates that future trends are opposite to past trends, the smaller the H value, the stronger the anti-persistence; $0.5 < H < 1$indicates that future trends are similar to past trends, the larger the H values, the stronger the persistence of the trend.

3.5. The cross-wavelet analysis

The cross-wavelet analysis, a new technique developed by Hudgins et al. (1993), is commonly used to explore the associations between two related time series. It is based on cross-spectrum analysis and a wavelet transform, and can reveal the variation characteristics and coupled oscillations of the selected series in the time–frequency domain (Torrence and Compo, 1998; Huang et al., 2016).

For two time series x_n and y_n, the cross-wavelet transform can be defined as $W^{XY} = W^X W^{Y*}$, where * indicates the complex conjugation. We then define the cross-wavelet power as $|W^{XY}|$ and the complex argument $\arg(W^{XY})$ can be interpreted as the local relative phase between x_n and y_n in time and frequency space. According to Torrence and Compo (1998), the theoretical distribution of the cross-wavelet power of the two time series with background power spectra $P_k{}^X$ and $P_k{}^Y$ can be expressed as follows:

$$D\left(\frac{|W_n^X(s) W_n^{Y*}(s)|}{\sigma_x \sigma_y} < p \right) = \frac{Z_v(p)}{v} \sqrt{P_k^X P_k^Y} \tag{19}$$

where $Z_v(p)$ indicates the confidence level related to the probability p for a probability distribution function identified by the square root of the result of two χ^2 distributions (Grinsted et al., 2004; Huang et al., 2016). The detailed codes can be freely downloaded from the website http://www.pol.ac.uk/home/research/waveletcoherence/.

3.6. Variance decomposition

Variance decomposition is useful for evaluating how shocks reverberate through a system. It determines how much of the forecast error variance for each of the variables can be explained by exogenous shocks to the other variables (Caselli, 2005). If we have the endogenous variable series y, and exogenous shocks x_i, $i = 1, 2, \ldots n$, the total variance can be calculated:

$$\mathrm{Var}(total) = \mathrm{Var}(\mathrm{y}) = \mathrm{Var}\left[\left(\mathrm{y} - \sum_{i=1}^{n} x_i \right) + \sum_{i=1}^{n} x_i \right] \tag{20}$$

Defining $g = \mathrm{y} - \sum_{i=1}^{n} x_i$ as the disturbance term, Eq. (20) can be restated as:

$$\mathrm{Var}(total) = \mathrm{Var}\left(g + \sum_{i=1}^{n} x_i \right) \quad i = 1, 2, \ldots n \tag{21}$$

The disturbance term g is related to the exogenous shocks x_i, and the variation associated with each shock can be calculated as:

$$\mathrm{Var}(x_i^{total}) = \mathrm{Var}(x_i) + \mathrm{cov}(g, x_i) \quad (i = 1, 2, \ldots n; j = 1, 2, \ldots n; and\ i \ne j) + \mathrm{cov}(x_i, x_j) \tag{22}$$

Thus the contribution of each exogenous shock to the endogenous variable is:

$$Contribution_{x_i} = \frac{\mathrm{Var}(x_i^{total})}{\mathrm{Var}(total)} \tag{23}$$

The relative contribution of each shock to the endogenous variable

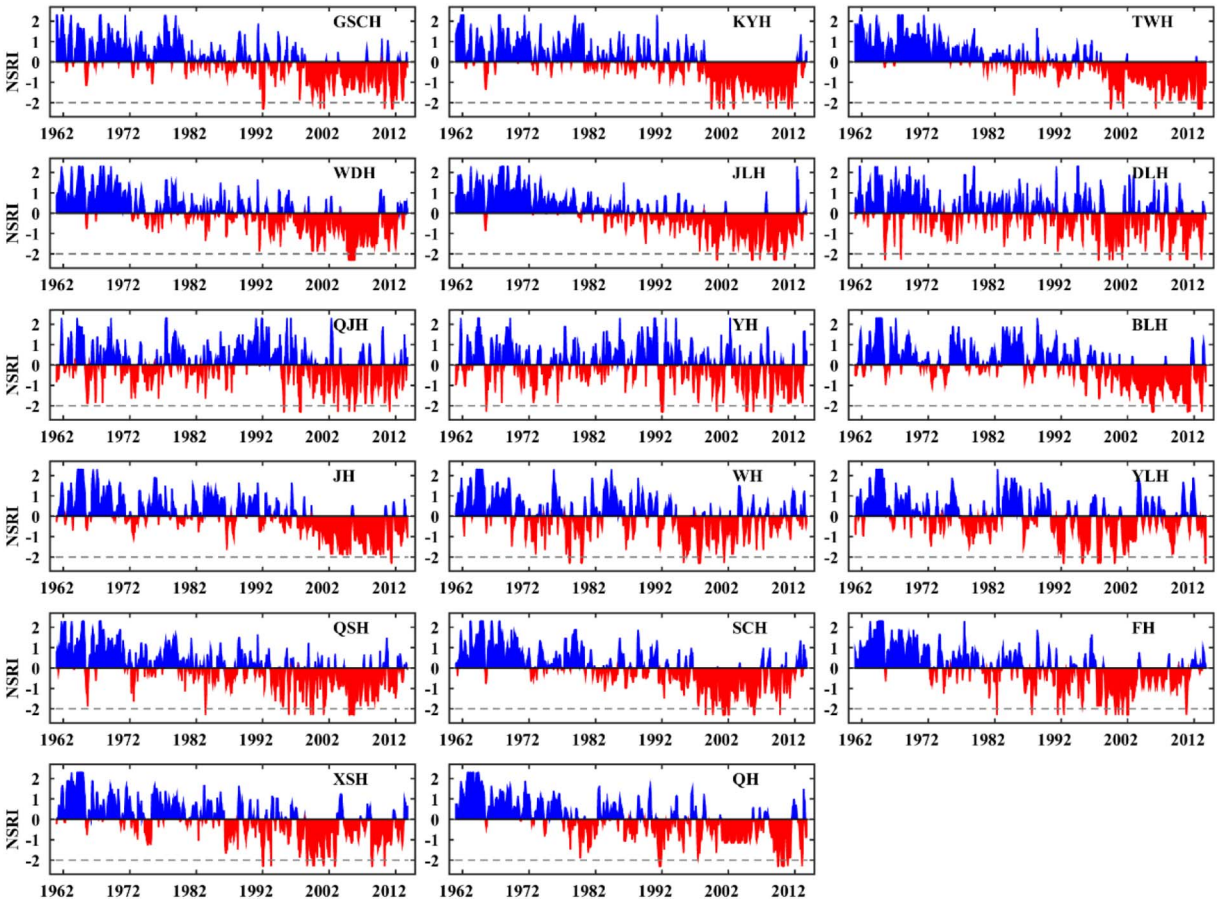

Fig. 2. Temporal patterns of hydrological drought identified through the NSRI-3 for 17 catchments on the Loess Plateau during the period 1961–2013. The red (blue) bars indicates the occurrence of hydrological drought (or no hydrological drought), respectively. The gray dotted line denotes the level corresponding to extreme severe hydrological drought. The acronyms in each subplot are listed in Table 1. (For interpretation of the references to color in this figure legend, the reader is referred to the web version of this article.)

represents the magnitude of the contribution, and can be calculated as:

$$Contribution_{x_i}^{relative} = \frac{(Contribution_{x_i})^2}{\sum_{i=1}^{n}(Contribution_{x_i})^2} \quad (24)$$

4. Results and discussion

4.1. Characteristics of historical short-term and long-term hydrological drought

Fig. 2 shows the temporal patterns of hydrological drought for 17 Loess Plateau catchments over the period 1961–2013, as identified by the NSRI-3 series according to the method introduced in Section 3.1. It can be seen that almost all 17 catchments had similar overall trends, tending towards drier hydrological conditions in more recent years. However, the details varied across catchments. For example, most catchments displayed three major trends across the entire time series: wetter conditions during the early years, alternating dry/wet conditions during the subsequent middle years, and drier conditions in the final years. Only Dali, Qingjian, Yanhe, and Weihe exhibited obvious alternating dry/wet conditions throughout the entire period (Fig. 2). This indicates that hydrological droughts occurred earlier in Dali, Qingjian, Yanhe and Weihe than in the other catchments and that the hydrological droughts in these catchments were more severe during the early period (1960s–1970s) than in other catchments, a result that is consistent with previous findings (Ren et al., 2016).

The temporal patterns of hydrological drought for the 17 catchments on the Loess Plateau over the period 1961–2013 as identified by the NSRI-12 series are shown in Fig. S1 in the Supplementary material. The results were similar to those obtained from the NSRI-3, and showed that hydrological drought occurred earlier in Dali, Qingjian, Yanhe, and Weihe than in the other catchments. Both the NSRI-3 and NSRI-12 indicated a reinforcement of drought severity since the 2000s for all catchments (Fig. 2 and Fig. S1 in the Supplementary materials). This is likely because statistically significant climatic drying has been identified in the region since the year 2000 (Feng et al., 2016). Moreover, water consumption increased markedly with the increases in vegetation cover and grain production during the 2000s (Feng et al., 2016). In addition, in order to increase water provision (McVicar et al., 2010), enhance carbon sequestration (Fu et al., 2011), and control water and soil loss (Ran, 2000), numerous ecological restoration measures have been implemented by the Chinese government over the last five decades (Liu et al., 2008). This means that the characteristics of the catchments on the Loess Plateau have undergone marked changes, especially since the 2000s (Liang et al., 2015; GY Gao et al., 2016). These changes resulted in low runoff coefficients (GY Gao et al., 2016) and thus led to the increase in severity of hydrological drought observed since the 2000s.

The mean hydrological drought intensity and duration for each of the 17 catchments plus the mean across all catchments are displayed in Table 2. It can be seen that, at the short-term scale, mean drought duration in Kuye and Jinghe was longer than 10 months and mean drought intensity was greatest in Yanhe (0.681) and Dali (0.653) (Table 2). Mean drought intensity and duration in Gushanchuan, Qingjian, and Qiushui were lower than the mean across all 17 catchments, whereas mean drought intensity and duration in Beiluo and Yiluo were greater than the overall catchment mean (Table 2). This indicates that, when considering the entire study period, hydrological

Table 2
Mean hydrological drought features at 17 catchments on the Loess Plateau. The bold font with superscript '*' ('**') indicates that both the intensity and duration were less than (greater than) the mean value across the entire plateau. The terms 'Short-term drought features' and 'Long-term drought features' indicate the characteristics of hydrological drought measured over 3-month and 12-month timescales, respectively.

Catchments	Short-term drought features		Long-term drought features	
	Intensity	Duration	Intensity	Duration
Gushanchuan	**0.532***	**6.94***	0.57	21.17
Kuye	0.582	10.08	0.556	43.33
Tuwei	0.591	9.46	0.562	18.29
Wuding	0.597	8.46	0.579	20.67
Jialu	0.621	6.65	0.55	44
Dali	0.653	4.47	0.59	13
Qingjian	**0.584***	**4.59***	0.588	13.44
Yanhe	0.681	4.29	0.561	12.6
Beiluo	**0.605****	**8.83****	0.519	32.25
Jinghe	0.539	14.25	0.488	26
Weihe	0.626	6.5	**0.557***	**11.82***
Yiluo	**0.632****	**8.77****	**0.561***	**9.92***
Qiushui	**0.579***	**5.41***	0.589	15.13
Sanchuan	0.577	8.36	**0.578****	**41.67****
Fenhe	0.639	7.21	0.595	16.86
Xinshui	0.608	6.94	0.575	12.5
Qinhe	0.622	6.19	0.538	18
Average	0.604	7.49	0.562	21.8

drought was most severe in Beiluo and Yiluo. At the long-term scale, mean drought duration was longest in Kuye, suggesting that this area tends to suffer from continuous hydrological drought. Similarly, taking the study period as a whole, drought intensity and duration were below the overall catchment mean in Weihe and Yiluo but above the catchment mean in Sanchuan (Table 2). This shows that hydrological drought was more severe in Sanchuan than in the other catchments. Overall, the risk of hydrological drought was high across all catchments studied. It is thus essential to investigate the detailed characteristics of hydrological drought in this region, such as seasonal and annual hydrological drought, trends and persistence, and linkages between the NSRI series and climate indices. We will discuss these characteristics in the following sections.

4.2. Trends and persistence in the seasonal and annual NSRI

The Loess Plateau has a typical continental monsoon climate, with distinct seasonality in the distributions of temperature and precipitation (Liang et al., 2015). Thus, evaluating hydrological drought at both seasonal and annual time scales may lead to a better understanding of the hydrological drought characteristics on the Loess Plateau. The results of the Mann-Kendall trend analysis of the seasonal and annual NSRI series for 1961–2013 are shown in Table 3. It can be seen that, for the spring NSRI series, there were statistically significant downward trends in 15 catchments, with Jialu (−0.615) showing the greatest downward trend ($p < 0.05$). Only Weihe and Yiluo did not show significant downward trends in the spring. For the summer NSRI series, all catchments had significant downward trends ($p < 0.05$), with the greatest downward trend in Sanchuan (−0.541) and the smallest downward trend in Qingjian (−0.23). The autumn NSRI series showed significant downward trends in all catchments except Qingjian (−0.183), with Tuwei (−0.565) exhibited the largest downward trend. For the winter NSRI series, there were downward trends ($p < 0.05$) in all catchments except Yanhe (0.206) and these trends were significant in all catchments except Dali (−0.046) and Qingjian (−0.105). The greatest winter downward trend was in Jialu. For the annual NSRI series, all catchments except Qingjian ($p < 0.05$) had highly significant ($p < 0.01$) downward trends, ranging from −0.241 (Qingjian) to −0.569 (Jialu). In short, the hydrological conditions in almost all catchments (except Yanhe in winter) tended to become drier at both

Table 3
Mann–Kendall trend analysis of the seasonal and annual NSRI series for 17 catchments on the Loess Plateau during the period 1961–2013. The superscripts '*' and '**' indicate significance at the 95% and 99% levels, respectively. The bold denotes the largest and smallest decreasing tendency of NSRI.

Catchment	Slope of NSRI (Ten years)				
	Spring	Summer	Autumn	Winter	Annual
Gushanchuan	−0.535**	−0.378**	−0.485**	−0.384**	−0.436**
Kuye	−0.563**	−0.407**	−0.483**	−0.464**	−0.5**
Tuwei	−0.563**	−0.5**	**−0.565****	−0.503**	−0.563**
Wuding	−0.556**	−0.405**	−0.504**	−0.5**	−0.518**
Jialu	**−0.615****	−0.469**	−0.544**	**−0.56****	**−0.569****
Dali	−0.388**	−0.26*	−0.31**	−0.046	−0.277**
Qingjian	−0.252*	**−0.23***	**−0.183**	−0.105	**−0.241***
Yanhe	−0.257*	−0.293**	−0.196*	**0.206***	−0.3**
Beiluo	−0.417**	−0.377**	−0.375**	−0.385**	−0.408**
Jinghe	−0.493**	−0.5**	−0.331**	−0.467**	−0.461**
Weihe	−0.179	−0.395**	−0.197*	−0.242*	−0.292**
Yiluo	**−0.144**	−0.284**	−0.241**	−0.205*	−0.248**
Qiushui	−0.377**	−0.533**	−0.464**	−0.522**	−0.472**
Sanchuan	−0.508**	**−0.541****	−0.455**	−0.545**	−0.462**
Fenhe	−0.525**	−0.415**	−0.415**	−0.475**	−0.429**
Xinshui	−0.45**	−0.362**	−0.443**	−0.42**	−0.455**
Qinhe	−0.44**	−0.428**	−0.41**	−0.395**	−0.415**

the seasonal and annual scales. The driest hydrological conditions in spring, summer, autumn, winter, and annually occurred in Jialu, Sanchuan, Tuwei, Jialu, and Jialu, respectively. In order to detail hydrological drought at the seasonal scale, the mean seasonal NSRI values were investigated and are shown in Fig. 3. The mean NSRI values exhibited clear downward trends in all 17 catchments; however, there was diversity in the individual characteristics of these downward trends. Most catchments showed a significant linear downward trend, except for Dali, Qingjian, Yanhe, Beiluo, Jinghe, Werihe, and Yiluo. The mean spring NSRI value was largest in the early period (1960s) and smallest in the 2000s for most catchments, for example Gushanchuan, Kuye, Tuwei, Jialu, Dali, Jinghe, and Weihe (Fig. 3). This indicates that hydrological drought trend in the spring in most catchments was more severe than other seasons in recent years.

We evaluated the potential changes in the seasonal and annual NSRI for these 17 catchments in the near future using a rescaled range analysis. As shown in Fig. 4, all Hurst index values for the seasonal and annual NSRI series during the period 1961–2013 were larger than 0.5. Combined with the results from the Mann–Kendall trend analysis shown in Table 3, we can conclude that the seasonal and annual NSRI series in all catchments are likely to exhibit downward trends in the near future, except for the winter NSRI series in Yanhe. In other words, there are likely to be upward trends in seasonal and annual hydrological drought in the near future in all 17 catchments except Yanhe, in which winter hydrological drought may decrease. These results are consistent with a previous study, which indicated that the Loess Plateau is expected to be warmer and drier in the future (Lü et al., 2012).

4.3. Contribution of changes in seasonal hydrological drought to changes in annual hydrological drought

The contributions of changes in seasonal hydrological drought to changes in annual hydrological drought were calculated according to the variance decomposition method introduced in Section 3.6. As shown in Fig. 5, the changes in summer NSRI series made the largest contribution to changes in the annual NSRI series in many catchments (e.g., Gushanchuan, Kuye, Tuwei, Wuding, Jialu, Dali, Yanhe, Beiluo, Jinghe, and Weihe), but not all. The dominant contribution from summer months is likely because precipitation is greater in the summer owing to the monsoon climate (Liang et al., 2015; Sun et al., 2015). When combined with the results in Fig. S2 in the Supplementary materials, we can see that the seasonal contributions had a clear spatial

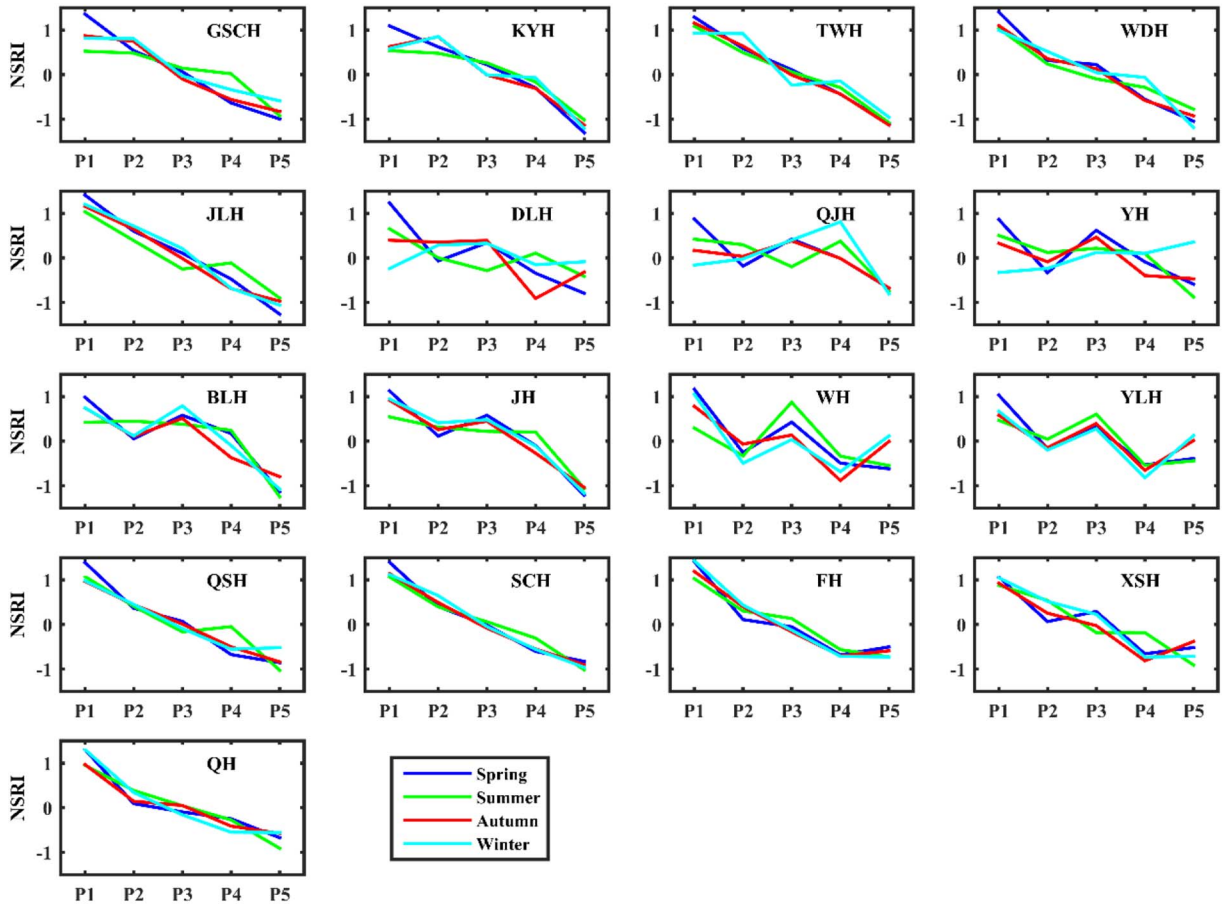

Fig. 3. The mean seasonal NSRI values for 17 catchments on the Loess Plateau during the last five decades. The catchment acronyms in each subplot are listed in Table 1. P1, P2, P3, P4, and P5 indicate 1961–1970, 1971–1980, 1981–1990, 1991–2000, and 2001–2013, respectively.

distribution: the changes in summer NSRI made the greatest contribution to changes in the annual NSRI in the west of the plateau but not in the east. This spatial disparity can be explained by the results of our previous research (Wu et al., 2017), which indicated that human activities have had a larger effect on runoff decline in the east of the plateau than the west. Fig. 6 shows this intuitively: the urban areas are much larger in the east of the Loess Plateau than the west, with twice as much urbanization per km^2. Furthermore, the degree of forestation was greater in the east than the west: forested areas covered 0.0155 km^2 per km^2 in the west but 0.0173 km^2 per km^2 in the east. The increase in plant coverage likely reduced the annual runoff. Bosch and Hewlett (1982) showed that a 10% increase in pine (broad-leaved forest) led to a 40 mm (25 mm) reduction in annual runoff. Leaves and trees can slow rain down as it falls to the ground, giving plant roots more time to absorb the water. Increased plant cover also enhances evaporation, improves the soil structure, and increases infiltration (Wu et al., 2017), with infiltration greatest for forest than for other land-use types (Bartens et al., 2008). Moreover, bark and leaf litter can significantly increase the roughness of the soil surface and thus retard runoff velocity (Xu, 2011). In short, all these factors contribute to reducing surface runoff.

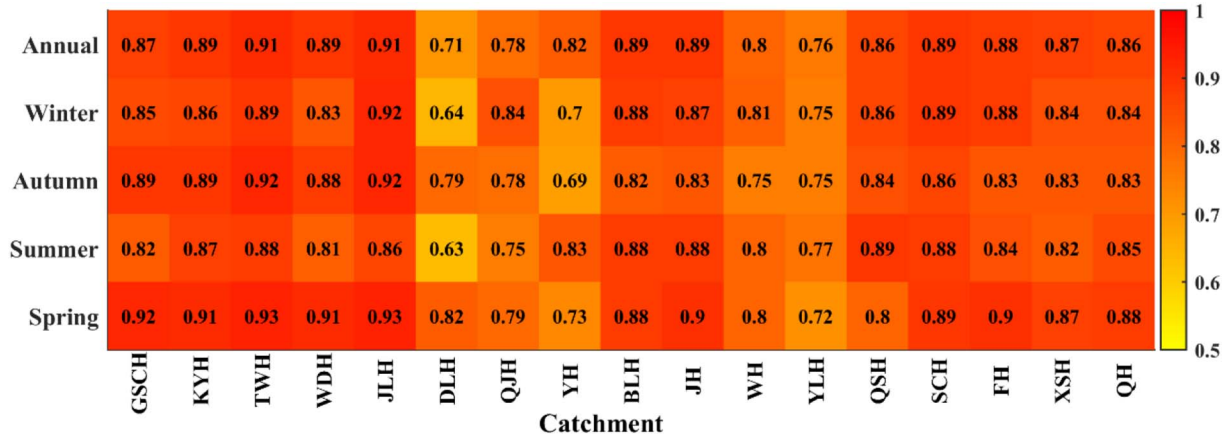

Fig. 4. Hurst index values for 17 catchments on the Loess Plateau, calculated from a rescaled range analysis. The catchment acronyms on the *x* axis are listed in Table 1.

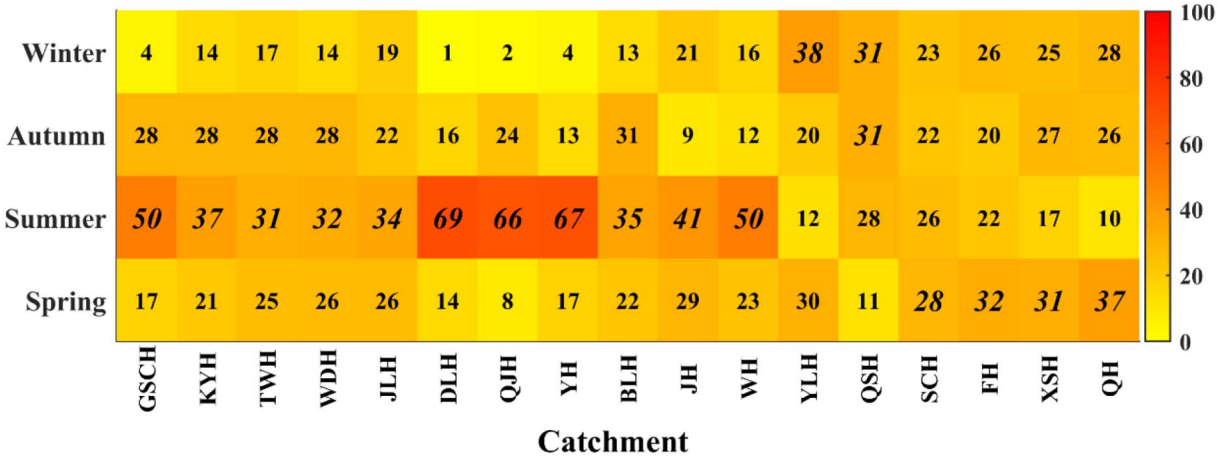

Fig. 5. Contributions (%) of the changes in seasonal NSRI series to the changes in annual NSRI series for 17 catchments on the Loess Plateau. The acronyms on the *x* axis are listed in Table 1. Italics denote the largest contributions to the annual NSRI series in each catchment.

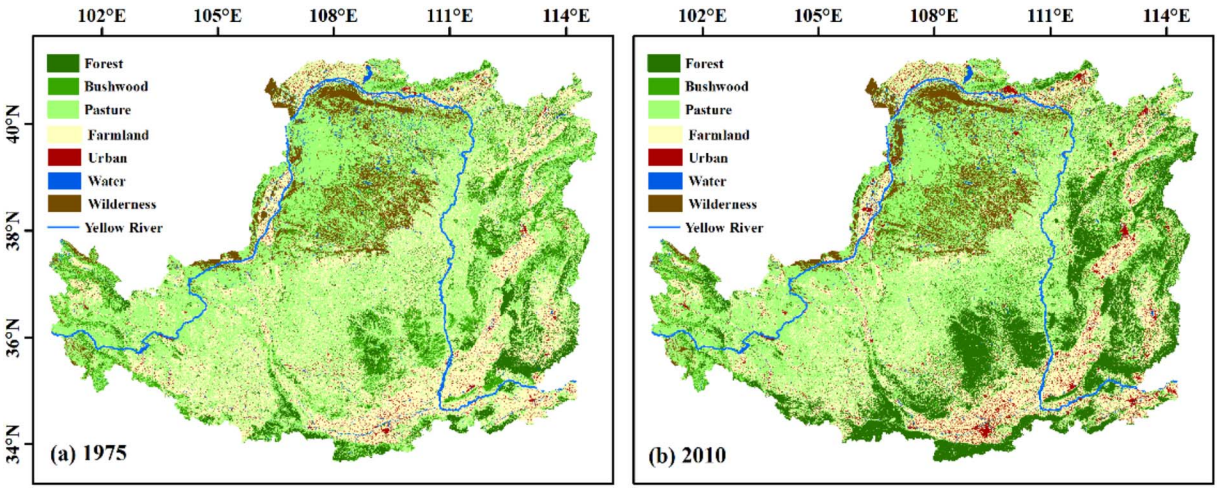

Fig. 6. Land use and land cover on the Loess Plateau in (a) 1975 and (b) 2010.

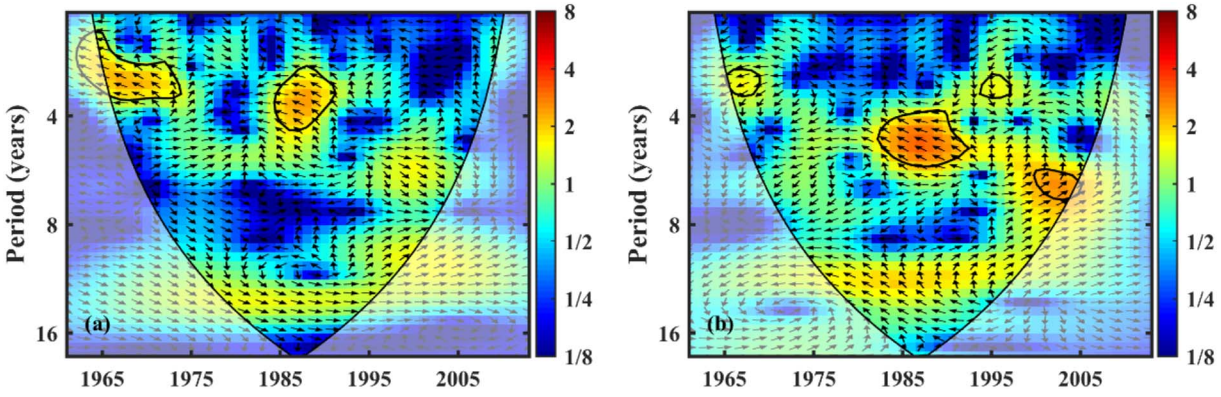

Fig. 7. Cross-wavelet transforms between ENSO events and the annual NSRI series for Kuye (a) and Yiluo (b). Black contours indicate regions where the significance reached the 95% confidence level against red noise. Arrows indicate the relative phase relationship, with anti-phase pointing left and in-phase pointing right. (For interpretation of the references to color in this figure legend, the reader is referred to the web version of this article.)

4.4. The correlations between seasonal/annual NSRI series and ENSO events

ENSO events are strongly associated with flood and drought events worldwide and exert a major influence on the climate at local and regional scales (Ryu et al., 2010; Fleig et al., 2011; Huang et al., 2015). Investigating the correlations between the ENSO index and hydrological drought may help to reveal the causes of hydrological drought from the perspective of climate change and could play an important role in mitigating the potential impacts of hydrological drought. Therefore, we used a cross-wavelet analysis to evaluate correlations between the NSRI series and the ENSO index at seasonal and annual scales on the Loess Plateau during the period 1961–2013. On the basis of mean precipitation, vegetation cover, aeolian sandy soil type, and

slope, as depicted by Liang et al. (2015), the Loess Plateau can be divided into two regions: the northwest region [characterized by lower mean precipitation (P < 440 mm), lower Leaf Area Index (LAI) (0.32–0.37 $m^2/m^2\ yr^{-1}$), an aeolian sandy soil type, and gentle slopes (2.6°–7.6°)] and a southeast region [characterized by relatively higher precipitation (485–530 mm), higher LAI (1.56 $m^2/m^2\ yr^{-1}$), loessal and heilu soils, and relatively steep slopes (8.9°–13.1°)]. To investigate the effects of ENSO events on hydrological drought in these different regions in detail, we selected Kuye and Yiluo as representative of the northwest and southeast regions of the Loess Plateau, because Kuye and Yiluo were most influenced by ENSO events in the northwest (Fig. S3) and southeast (Fig. S4) regions of the Loess Plateau, respectively.

The cross-wavelet transforms at the annual scale for 1961–2013 are shown in Fig. 7. It can clearly be seen that ENSO events had a strong effect on the annual NSRI series in both Kuye and Yiluo, indicating that ENSO events strongly influence the evolutionary characteristics of hydrological drought in these two catchments. As shown in Fig. 7(a), ENSO events were significantly negatively correlated with the annual NSRI in Kuye with a signal of 2–3 years in 1961–1974 and a signal of 3–5 years in 1984–1991 (95% confidence level). Similarly, ENSO events were significantly negatively correlated with the annual NSRI series in Yiluo with a signal of 2–3 years 1965–1969 and 1993–1997, and a signal of 4–6 years in 1982–1992 (95% confidence level). In addition, ENSO events were significantly positively correlated with the annual NSRI in Yiluo with a signal of 6–7 years in 2000–2005 (95% confidence level). In general, ENSO events are closely associated with annual hydrological drought on the Loess Plateau, and the impact of ENSO events is stronger in the south than in the north (Figs. 7, S3 and S4). The Loess Plateau is notably affected by the monsoon climate, with more and heavier rainfall in the south of the plateau than in the north (Xie et al., 2007; Miao et al., 2015; Ashouri et al., 2015). However, human activities are also more intensive in the south of the plateau than in the north (owing to increased agriculture and urban water consumption, etc.) (Fig. 6), resulting in a significant and ongoing decrease in runoff that exacerbate the hydrological drought.

We also investigated the cross-wavelet transforms between the seasonal NSRI series and ENSO events for these two catchments, as illustrated in Figs. 8 and 9. ENSO events had a strong effect on the seasonal NSRI series in Kuye (Fig. 8). Specifically, the spring NSRI series was significantly negatively correlated with ENSO events with a 2–3 year period in 1966–1972 and 1977–1985 (95% confidence level). The summer NSRI series was significantly negatively correlated with ENSO events with a 2–4 year period in 1963–1971 and with a 3–4 year period in 1983–1989 (95% confidence level). The autumn NSRI series was also significantly negatively correlated with the ENSO index with a 1–4 year period in 1962–1974 and a 3–4 year period in 1992–1997 (95% confidence level). The winter NSRI series was significantly positively correlated with ENSO events with a signal of 2–4 years in 1964–1970, but was significantly negatively correlated with ENSO events with a signal of 5–6 years in 1974–1982 (95% confidence level). The ENSO index also had strong effects on all seasonal NSRI series in Yiluo, with the largest effect on the spring NSRI series (Fig. 9). In particular, ENSO events had a significant negative correlation with the spring NSRI series with a period of 4–6 years in 1980–1991 and also a significant positive correlation with a period of 2–4 years in 1964–1972 [Fig. 9(a)]. The summer NSRI series was significantly negatively correlated with the ENSO index with a signal of 4–6 years in 1989–2000, and significantly positively correlated with the ENSO index with a signal of 2–5 years in 1984–1997 (95% confidence level) [Fig. 9(b)]. The ENSO index was significantly negatively correlated with the autumn NSRI series with a signal of 4–6 years in 1982–1994 (95% confidence level) [Fig. 9(c)]. The winter NSRI series was significantly positively correlated with the ENSO index with a signal of 3–4 years in 1965–1972 but significantly negatively correlated with the ENSO index with a signal of 4–5 years in 1974–1989, (both at the 95% confidence level) [Fig. 9(d)]. Comparing Figs. 8 and 9, it can be seen that the impact of the ENSO index on the seasonal NSRI series was stronger at Yiluo than at Kuye, indicating that the impact of ENSO events on seasonal hydrological drought is stronger in Yiluo (southeast Loess Plateau) than in Kuye (northwest Loess Plateau).

4.5. Discussion

In this study, we assessed the evolutionary characteristics of hydrological drought on the Loess Plateau. We conclude that the plateau has been suffering ongoing hydrological drought over the last five decades, and that this trend will continue in the future. Many other studies have investigated the characteristics of hydrological drought in regions all over the world. Tabari et al. (2013) showed northwestern Iran suffered from extreme hydrological droughts between 1975 and 2009, with extreme droughts occurring most frequently from 1997 to 2009. Wanders and Wada (2015) investigated the projected effects of human and climate factors on 21st-century hydrological drought at the global scale, and predict severe hydrological drought characteristics with large regions expected to suffer from the negative impact of climate change on drought deficit volumes. Wada et al. (2013) evaluated hydrological drought worldwide over the last fifty years, and noted a decrease in local and downstream streamflow in Europe, North America, and Asia, which subsequently intensified the magnitude of hydrological droughts by 10–500%. Thus, hydrological drought occurs all over the world against a background of global warming and intensive human activities; the results of this study concur with these previews studies.

However, the methods and hydrological drought indices used vary from study to study, and there are pros and cons associated with each index. Most drought indices are derived by fitting a parametric distribution to the data, whereas we use a nonparametric standardized runoff index to characterize hydrological drought. The attractive feature of the hydrological drought index used in this study is that it is statistically comparable and spatially and temporally consistent, which means that the methodology can be applied to different climate and land-surface variables (precipitation, soil moisture, runoff, etc.) without having to assume the existence of representative parametric distributions (Farahmand and AghaKouchak, 2015; Yang et al., 2017a). In addition, empirical distributions (nonparametric distribution function) are based on data set ranks rather than actual values. Drought analysis is based on relative departures from the climatology, thus empirical distributions are appropriate. However, the sample size needs to be relatively large. For very short data sets (e.g. fewer than ten measurements), an empirical distribution can lead to misleading probabilities (Farahmand and AghaKouchak, 2015).

5. Conclusions

Among all drought types, hydrological drought is the most important and the most in need of further research because of our high dependence on water resources. Depicting the evolutionary characteristics of hydrological drought in detail may help obtain a better understanding of drought mechanisms and mitigate the impact of droughts. In this study, the main conclusions are as follows:

(1) Almost all catchments exhibited downward trends in the NSRI, except the winter NSRI series in Yanhe. The greatest downward trends for the spring, summer, autumn, winter, and annual NSRI series were in Jialu (−0.615), Sanchuan (−0.541), Tuwei (−0.541), Jialu (−0.56), and Jialu (−0.569), respectively. This indicates that the driest hydrological conditions in spring, summer, autumn, winter, and annually occurred in Jialu, Sanchuan, Tuwei, Jialu, and Jialu, respectively.
(2) The mean spring NSRI in most catchments was largest in the 1960s and smallest in the 2000s for almost all seasonal NSRI series. This indicates that trend of hydrological drought in the spring was more

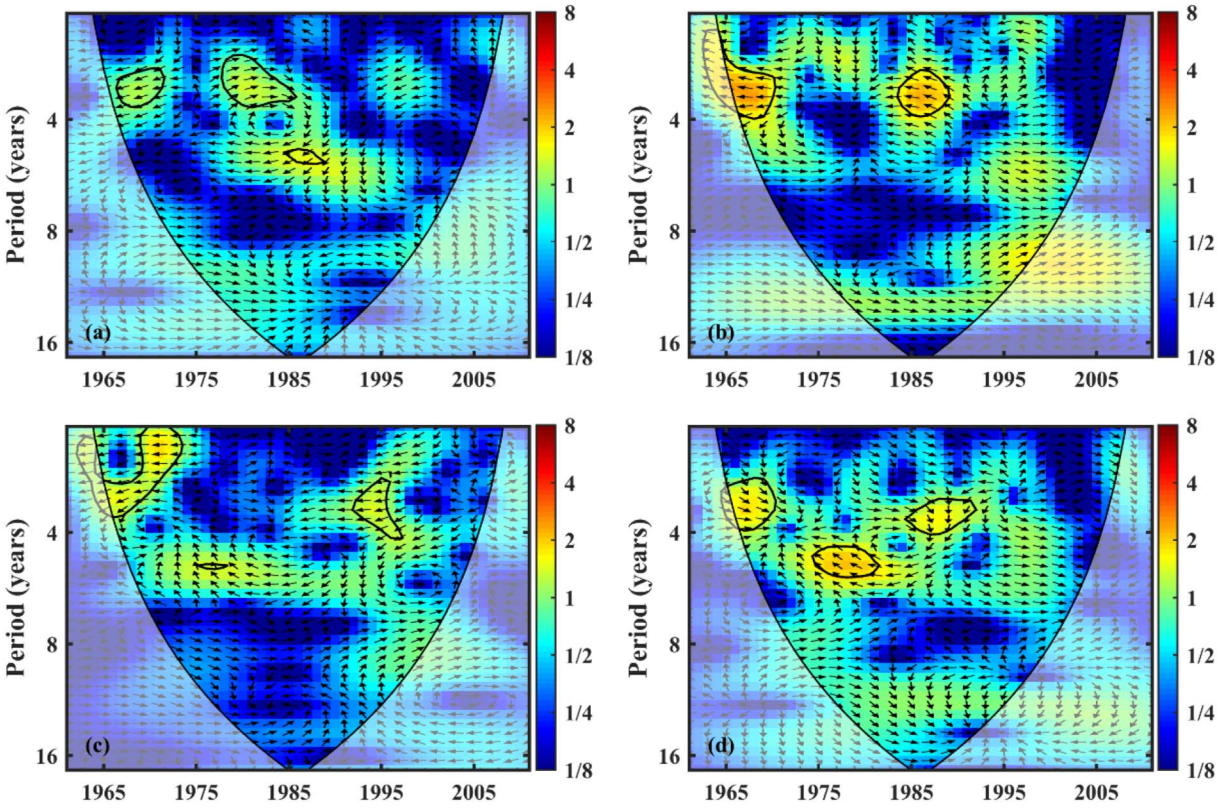

Fig. 8. Cross-wavelet transforms between ENSO events and the seasonal NSRI series for Kuye. (a) Spring. (b) Summer. (c) Autumn. (d) Winter. Black contours indicate regions where the significance reached the 95% confidence level against red noise. Arrows indicate the relative phase relationship, with anti-phase pointing left and in-phase pointing right. (For interpretation of the references to color in this figure legend, the reader is referred to the web version of this article.)

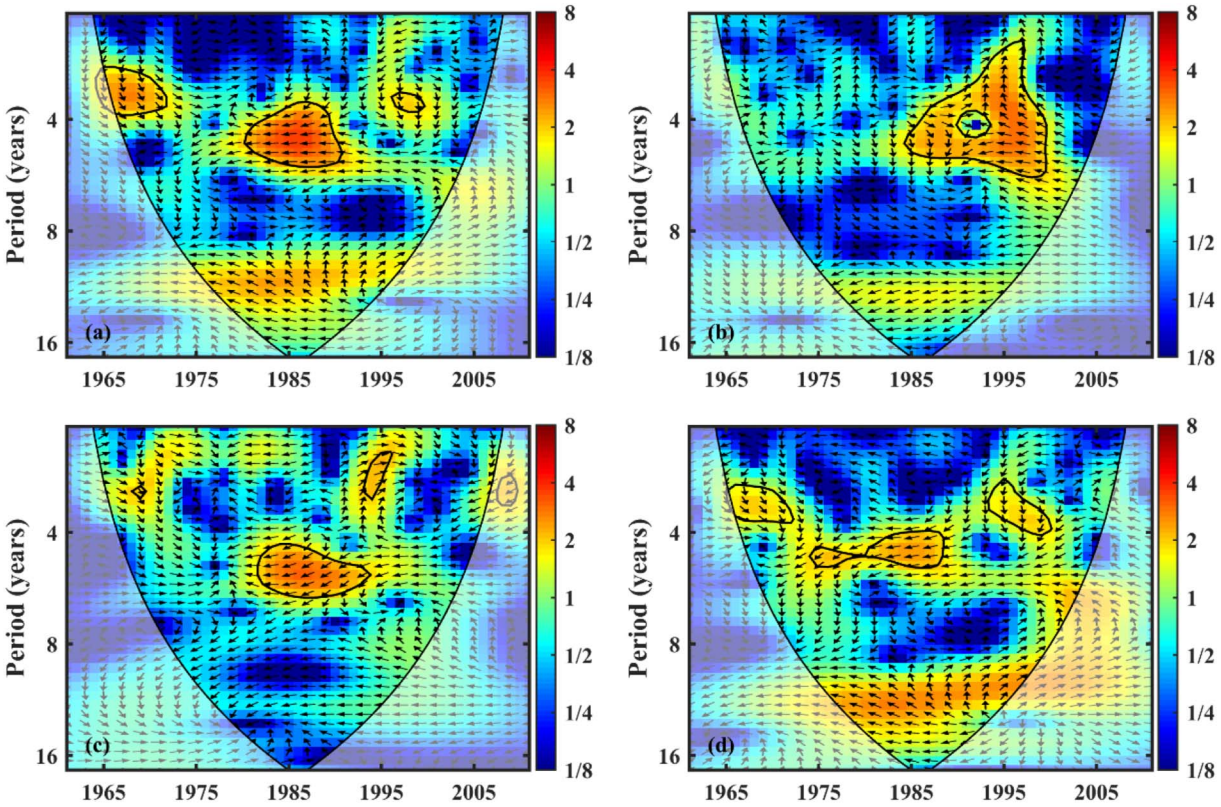

Fig. 9. Cross-wavelet transforms between ENSO events and the seasonal NSRI series for Yiluo. (a) Spring. (b) Summer. (c) Autumn. (d) Winter. Black contours indicate regions where the significance reached the 95% confidence level against red noise. Arrows indicate the relative phase relationship, with anti-phase pointing left and in-phase pointing right. (For interpretation of the references to color in this figure legend, the reader is referred to the web version of this article.)

severe than that in other seasons in recent years.
(3) Seasonal and annual hydrological drought is likely to increase in the near future in all 17 catchments except for Yanhe, where winter hydrological drought is predicted to decrease.
(4) There was a clear spatial distribution of the seasonal contributions to annual hydrological drought: the summer NSRI made the greatest contribution to hydrological drought in the west of the Loess Plateau but not in the east.
(5) ENSO events are closely associated with both annual and seasonal hydrological droughts on the Loess Plateau. The impact of ENSO events was stronger in the southeast of the plateau than the northwest at both seasonal and annual scales.

In summary, this study thoroughly investigated the characteristics of hydrological drought at both seasonal and annual scales and revealed the correlations between ENSO events and hydrological drought. These results may be useful in predicting and mitigating future hydrological drought on the Loess Plateau.

Acknowledgements

This research was supported by the National Natural Science Foundation of China (No. 91547118; No. 41622101), the Fundamental Research Funds for the Central Universities, and the State Key Laboratory of Earth Surface Processes and Resource Ecology.

Appendix A. Supplementary data

Supplementary data to this article can be found online at https://doi.org/10.1016/j.gloplacha.2017.12.006.

References

Ashouri, H., Hsu, K.L., Sorooshian, S., Braithwaite, D.K., Knapp, K.R., Cecil, L.D., Nelson, B.R., Prat, O.P., 2015. PERSIANN-CDR daily precipitation climate data record from multisatellite observations for hydrological and climate studies. Bull. Am. Meteorol. Soc. 96 (1), 69–83.
Bartens, J., Day, S.D., Harris, J.R., Dove, J.E., Wynn, T.M., 2008. Can urban tree roots improve infiltration through compacted subsoils for stormwater management? J. Environ. Qual. 37 (6), 2048–2057.
Bosch, J.M., Hewlett, J.D., 1982. A review of catchment experiments to determine the effect of vegetation changes on water yield and evapo-transpiration. J. Hydrol. 55 (1–4), 3–23.
Caselli, F., 2005. Accounting for cross-country income differences. In: Handbook of Economic Growth, (North Holland, New York).
Dracup, J.A., Lee, K.S., Paulson, E.G., 1980. On the definition of droughts. Water Resour. Res. 16 (2), 297–302.
Farahmand, A., AghaKouchak, A., 2015. A generalized framework for deriving non-parametric standardized drought indicators. Adv. Water Resour. 76, 140–145.
Feng, X.M., Cheng, W., Fu, B.J., Lu, Y.H., 2016. The role of climatic and anthropogenic stresses on long-term runoff reduction from the Loess Plateau, China. Sci. Total Environ. 571, 688–698.
Fleig, A.K., Tallaksen, L.M., Hisdal, H., Hannah, D.M., 2011. Regional hydrological drought in north-western Europe: linking a new regional drought area index with weather types. Hydrol. Process. 25 (7), 1163–1179.
Fu, B.J., Liu, Y., Lu, Y.H., He, C.S., Zeng, Y., Wu, B.F., 2011. Assessing the soil erosion control service of ecosystems change in the Loess Plateau of China. Ecol. Complex. 8 (4), 284–293.
Gao, Y., Zhu, B., He, N.P., Yu, G.R., Wang, T., Chen, W.L., Tian, J., 2014a. Phosphorus and carbon competitive sorption-desorption and associated non-point loss respond to natural rainfall events. J. Hydrol. 517, 447–457.
Gao, Y., Zhu, X.J., Yu, G.R., He, N.P., Wang, Q.F., Tian, J., 2014b. Water use efficiency threshold for terrestrial ecosystem carbon sequestration under afforestation in China. Agric. For. Meteorol. 195–196, 32–37.
Gao, G.Y., Fu, B.J., Wang, S., Liang, W., Jiang, X.H., 2016. Determining the hydrological responses to climate variability and land use/cover change in the Loess Plateau with the Budyko framework. Sci. Total Environ. 557, 331–342.
Gao, Y., Yu, G.R., Yang, T.T., Jia, Y.L., He, N.P., Zhuang, J., 2016. New insight into global blue carbon estimation under human activity in land-sea interaction area: a case study of China. Earth Sci. Rev. 159, 36–46.
Gocic, M., Trajkovic, S., 2013. Analysis of precipitation and drought data in Serbia over the period 1980–2010. J. Hydrol. 494, 32–42.
Gringorten, I.I., 1963. A plotting rule for extreme probability paper. J. Geophys. Res. 68 (3), 813–814.
Grinsted, A., Moore, J.C., Jevrejeva, S., 2004. Application of the cross wavelet transform and wavelet coherence to geophysical time series. Nonlinear Process. Geophys. 11 (5–6), 561–566.
Hao, Z.C., AghaKouchak, A., 2013. Multivariate standardized drought index: a parametric multi-index model. Adv. Water Resour. 57, 12–18.
Huang, S.Z., Huang, Q., Chang, J.X., Zhu, Y.L., Leng, G.Y., Xing, L., 2015. Drought structure based on a nonparametric multivariate standardized drought index across the Yellow River basin, China. J. Hydrol. 530, 127–136.
Huang, S.Z., Huang, Q., Chang, J.X., Leng, G.Y., 2016. Linkages between hydrological drought, climate indices and human activities: a case study in the Columbia River basin. Int. J. Climatol. 36 (1), 280–290.
Hudgins, L., Friehe, C.A., Mayer, M.E., 1993. Wavelet transforms and atmospheric-turbulence. Phys. Rev. Lett. 71 (20), 3279–3282.
Hurst, H., 1951. Long term storage capacity of reservoirs. Trans. Am. Soc. Civ. Eng. 116, 770–799.
Keyantash, J.A., Dracup, J.A., 2004. An aggregate drought index: assessing drought severity based on fluctuations in the hydrologic cycle and surface water storage. Water Resour. Res. 40 (9). http://dx.doi.org/10.1029/2003wr002610.
Kong, D.X., Miao, C.Y., Wu, J.W., Duan, Q.Y., 2016. Impact assessment of climate change and human activities on net runoff in the Yellow River Basin from 1951 to 2012. Ecol. Eng. 91, 566–573.
Liang, W., Bai, D., Wang, F.Y., Fu, B.J., Yan, J.P., Wang, S., Yang, Y.T., Long, D., Feng, M.Q., 2015. Quantifying the impacts of climate change and ecological restoration on streamflow changes based on a Budyko hydrological model in China's Loess Plateau. Water Resour. Res. 51 (8), 6500–6519.
Liu, J.G., Li, S.X., Ouyang, Z.Y., Tam, C., Chen, X.D., 2008. Ecological and socioeconomic effects of China's policies for ecosystem services. Proc. Natl. Acad. Sci. U. S. A. 105 (28), 9477–9482.
Liu, X., Liu, C., Luo, Y., Zhang, M., Xia, J., 2012. Dramatic decrease in streamflow from the headwater source in the central route of China's water diversion project: climatic variation or human influence? 117 (D6). http://dx.doi.org/10.1029/2011JD016879.
Liu, X., Liu, C., Brutsaert, W., 2016. Regional evaporation estimates in the eastern monsoon regions of China: assessment of a nonlinear formulation of the complementary principle. Water Resour. Res. 52, 9511–9521.
Liu, Z.P., Wang, Y.Q., Shao, M.G., Jia, X.X., Li, X.L., 2016. Spatiotemporal analysis of multiscalar drought characteristics across the Loess Plateau of China. J. Hydrol. 534, 281–299.
Liu, X., Yang, T., Hsu, K., Liu, C., Sorooshian, S., 2017. Evaluating the streamflow simulation capability of PERSIANN-CDR daily rainfall products in two river basins on the Tibetan Plateau. Hydrol. Earth Syst. Sci. 21 (1), 169–181.
Lü, Y.H., Fu, B.J., Feng, X.M., Zeng, Y., Liu, Y., Chang, R.Y., Sun, G., Wu, B.F., 2012. A policy-driven large scale ecological restoration: quantifying ecosystem services changes in the Loess Plateau of China. PLoS One 7 (2). http://dx.doi.org/10.1371/journal.pone.0031782.
McKee, T.B., Doesen, N.J., Kleist, J., 1993. The relationship of drought frequency and duration to time scales. In: Preprints, 8th Conference on Applied Climatology, 17–22 January, Anaheim, California, USA, pp. 179–184.
McVicar, T.R., Van Niel, T.G., Li, L.T., Wen, Z.M., Yang, Q.K., Li, R., Jiao, F., 2010. Parsimoniously modelling perennial vegetation suitability and identifying priority areas to support China's re-vegetation program in the Loess Plateau: matching model complexity to data availability. For. Ecol. Manag. 259 (7), 1277–1290.
Miao, C.Y., Ni, J.R., Borthwick, A.G.L., Yang, L., 2011. A preliminary estimate of human and natural contributions to the changes in water discharge and sediment load in the Yellow River. Glob. Planet. Chang. 76 (3–4), 196–205.
Miao, C.Y., Ashouri, H., Hsu, K.L., Sorooshian, S., Duan, Q.Y., 2015. Evaluation of the PERSIANN-CDR daily rainfall estimates in capturing the behavior of extreme precipitation events over China. J. Hydrometeorol. 16 (3), 1387–1396.
Miao, C.Y., Kong, D.X., Wu, J.W., Duan, Q.Y., 2016. Functional degradation of the water-sediment regulation scheme in the lower Yellow River: spatial and temporal analyses. Sci. Total Environ. 551, 16–22.
Mishra, A.K., Singh, V.P., 2010. A review of drought concepts. J. Hydrol. 391 (1–2), 204–216.
Ran, D.C., 2000. Summary on runoff and sedimentation variation research from Hekouzhen to Longmen in the middle reaches of the Yellow River. J. Sediment. Res. 3, 72–81.
Ren, L.L., Shen, H.R., Yuan, F., Zhao, C.X., Yang, X.L., Zheng, P.L., 2016. Hydrological drought characteristics in the Weihe catchment in a changing environment. Adv. Water Sci. 27 (4), 492–500.
Ryu, J.H., Svoboda, M.D., Lenters, J.D., Tadesse, T., Knutson, C.L., 2010. Potential extents for ENSO-driven hydrologic drought forecasts in the United States. Clim. Chang. 101 (3–4), 575–597.
Sadeghipour, J., Dracup, J.A., 1985. Regional frequency-analysis of hydrologic multiyear droughts. Water Resour. Bull. 21 (3), 481–487.
Shafer, B.A., Dezman, L.E., 1982. Development of a Surface Water Supply Index (SWSI) to assess the severity of drought conditions in snowpack runoff areas. In: Proceedings of the Western Snow Conference. Colorado State University, Fort Collins, CO, pp. 164–175.
Shi, P., Ma, X.X., Chen, X., Qu, S.M., Zhang, Z.C., 2013. Analysis of variation trends in precipitation in an upstream catchment of Huai River. Math. Probl. Eng. http://dx.doi.org/10.1155/2013/929383.
Shukla, S., Wood, A.W., 2008. Use of a standardized runoff index for characterizing hydrologic drought. Geophys. Res. Lett. 35 (2). http://dx.doi.org/10.1029/2007gl032487.
Sun, Q.H., Miao, C.Y., Duan, Q.Y., Wang, Y.F., 2014. Variations in global temperature and precipitation for the period of 1948 to 2010. Environ. Monit. Assess. 186 (9), 5663–5679.
Sun, Q.H., Miao, C.Y., Duan, Q.Y., Wang, Y.F., 2015. Temperature and precipitation

changes over the Loess Plateau between 1961 and 2011, based on high-density gauge observations. Glob. Planet. Chang. 132, 1–10.
Tabari, H., Nikbakht, J., Talaee, P.H., 2013. Hydrological drought assessment in northwestern Iran based on Streamflow Drought Index (SDI). Water Resour. Manag. 27 (1), 137–151.
Talaee, P.H., Tabari, H., Ardakani, S.S., 2014. Hydrological drought in the west of Iran and possible association with large-scale atmospheric circulation patterns. Hydrol. Process. 28 (3), 764–773.
Tallaksen, L.M., Lanen, V., J., H.A., 2004. Hydrological drought: processes and estimation methods for streamflow and groundwater. Dev. Water Sci. 48, 579.
Torrence, C., Compo, G.P., 1998. A practical guide to wavelet analysis. Bull. Am. Meteorol. Soc. 79 (1), 61–78.
Van Lanen, H.A.J., Fendekova, M., Kupczyk, E., Kasprzyk, A., Pokojski, W., 2004. Flow generating processes. In: Tallaksen, L.M., Van Lanen, H.A.J. (Eds.), Hydrological Drought, Processes and Estimation Methods for Streamflow and Groundwater, Chapter 3. Dev. Water Sci. 48. pp. 53–96 (Amsterdam).
Van Loon, A.F., Laaha, G., 2015. Hydrological drought severity explained by climate and catchment characteristics. J. Hydrol. 526, 3–14.
Vicente-Serrano, S.M., Lopez-Moreno, J.I., Begueria, S., Lorenzo-Lacruz, J., Azorin-Molina, C., Moran-Tejeda, E., 2012. Accurate computation of a streamflow drought index. J. Hydrol. Eng. 17 (2), 318–332.
Wada, Y., van Beek, L.P.H., Wanders, N., Bierkens, M.F.P., 2013. Human water consumption intensifies hydrological drought worldwide. Environ. Res. Lett. 8 (3). http://dx.doi.org/10.1088/1748-9326/8/3/034036.
Wanders, N., Wada, Y., 2015. Human and climate impacts on the 21st century hydrological drought. J. Hydrol. 526, 208–220.
Wang, Y., Feng, Q., Chen, L.J., Yu, T.F., 2013. Significance and effect of ecological rehabilitation project in inland river basins in Northwest China. Environ. Manag. 52 (1), 209–220.
Wang, L.N., Zhu, Q.K., Zhao, W.J., Zhao, X.K., 2015. The drought trend and its relationship with rainfall intensity in the Loess Plateau of China. Nat. Hazards 77 (1), 479–495.
Wang, Y.X., Li, J.Z., Feng, P., Chen, F.L., 2015. Effects of large-scale climate patterns and human activities on hydrological drought: a case study in the Luanhe River basin, China. Nat. Hazards 76 (3), 1687–1710.
Wang, S., Fu, B.J., CHen, H.B., Liu, Y., 2017. Regional development boundary of China's Loess Plateau: water limit and land shortage. Land Use Policy. http://dx.doi.org/10.1016/j.landusepol.2017.03.003.
Wu, J., Miao, C., Wang, Y., Duan, Q., Zhang, X., 2017. Contribution analysis of the long-term changes in seasonal runoff on the Loess Plateau, China, using eight Budyko-based methods. J. Hydrol. 545, 263–275.
Xie, P.P., Yatagai, A., Chen, M.Y., Hayasaka, T., Fukushima, Y., Liu, C.M., Yang, S., 2007. A gauge-based analysis of daily precipitation over East Asia. J. Hydrometeorol. 8 (3), 607–626.
Xu, J.X., 2011. Variation in annual runoff of the Wudinghe River as influenced by climate change and human activity. Quat. Int. 244 (2), 230–237.
Yang, T., Asanjan, A.A., Faridzad, M., Hayatbini, N., Gao, X., Sorooshian, S., 2017a. An enhanced artificial neural network with a shuffled complex evolutionary global optimization with principal component analysis. Inf. Sci. 418–419, 302–316.
Yang, T., Asanjan, A.A., Welles, E., Gao, X., Sorooshian, S., Liu, X., 2017b. Developing reservoir monthly inflow forecasts using artificial intelligence and climate phenomenon information. Water Resour. Res. 53 (4), 2786–2812.
Yang, T., Tao, Y., Li, J., Zhu, Q., Su, L., He, X., Zhang, X., 2017c. Multi-criterion model ensemble of CMIP5 surface air temperature over China. Theor. Appl. Climatol. http://dx.doi.org/10.1007/s0070.
Yuan, X., Wood, E.F., 2013. Multimodel seasonal forecasting of global drought onset. Geophys. Res. Lett. 40 (18), 4900–4905.
Yuan, X., Wang, R.Y., Yang, J.H., Yue, P., Lu, D.R., Xiao, G.J., Wang, Y., Liu, L.C., 2016. An experimental seasonal hydrological forecasting system over the Yellow River basin - part 1: understanding the role of initial hydrological conditions. Hydrol. Earth Syst. Sci. 20 (6), 2437–2451.
Yue, S., Pilon, P., Cavadias, G., 2002. Power of the Mann-Kendall and Spearman's rho tests for detecting monotonic trends in hydrological series. J. Hydrol. 259 (1–4), 254–271.
Zargar, A., Sadiq, R., Naser, B., Khan, F.I., 2011. A review of drought indices. Environ. Rev. 19, 333–349.
Zhang, L., Schwärzel, K. (Eds.), 2017. Multifunctional Land-use Systems for Managing the Nexus of Environmental Resources, http://dx.doi.org/10.1007/978-3-319-54957-62.
Zhao, X.N., Wu, P., 2013. Meteorological drought over the Chinese Loess Plateau: 1971–2010. Nat. Hazards 67 (2), 951–961.